Self-archival version of the article published in Journal of Environmental Management:
R. Gueccia, S. Randazzo, D. Chillura Martino, A. Cipollina, G. Micale, 2019. Experimental investigation and modeling of diffusion dialysis for HCl recovery from waste pickling solution. Journal of Environmental Management 235, 202-212.
https://doi.org/10.1016/j.jenvman.2019.01.028

Experimental investigation and modeling of diffusion dialysis for HCl recovery from waste pickling solution

R. Gueccia [a], S. Randazzo [a], D. Chillura Martino [b], A. Cipollina [a], G. Micale [a]

[a]Dipartimento dell'Innovazione Industriale e Digitale - Ingegneria Chimica, Gestionale, Informatica, Meccanica, Università di Palermo – Viale delle Scienze ed.6, 90128 Palermo, Italy.
[b]Dipartimento di Scienze e Tecnologie Biologiche, Chimiche e Farmaceutiche, Università di Palermo – Viale delle Scienze ed.17, 90128 Palermo, Italy.
[*]Corresponding Author. e-mail: serena.randazzo@unipa.it

Abstract

Hydrochloric acid recovery from pickling solutions was studied by employing a batch diffusion dialysis (DD) laboratory test-rig equipped with Fumasep membranes. The effect of main operating parameters such as HCl concentration (0.1-3 M) and the presence of Fe^{2+} (up to 150 g/l) was investigated to simulate the system operation with real industrial streams. The variation of HCl, Fe^{2+} and water flux was identified. When only HCl is present, a recovery efficiency of 100% was reached. In the presence of $FeCl_2$, higher acid recovery efficiencies, up to 150%, were observed due to the so-called "salt effect", which promotes the passage of acid even against its concentration gradient. A 7% leakage of $FeCl_2$ was detected in the most severe conditions. An original analysis on water flux in DD operation has indicated that osmotic flux prevails at low HCl concentrations, while a dominant "drag flux" in the opposite direction is observed for higher HCl concentrations.

A comprehensive mathematical model was developed and validated with experimental data. The model has a time and space distributed-parameters structure allowing to effectively simulate steady-state and transient batch operations, thus providing an operative tool for the design and optimization of DD units.

Keywords: Pickling process; Diffusion dialysis; Modeling; Industrial waste recovery; AEM.

1. Introduction

The pickling process is an essential step in steel manufacturing industry. During the pickling treatment, ferrous ions are released in solution, after being complexed in $FeCl_2$, reaching concentrations up to 200 g/l, while the acid concentration decreases by 75-85%. A pickling bath in this condition is considered spent (Regel-Rosocka, 2010) and provides low pickling rate, thus requiring to be replaced. Disposal of the industrial pickling waste strongly affects the hot-dip galvanizing industries economics and environmental footprint. Thus, the recovery of acid is one of the most beneficial steps to enhance the process sustainability.

Several techniques have been proposed to reuse spent pickling liquor by recovering the free acid (e.g. by membrane technologies), or by regenerating the acid (e.g. by pyrohydrolysis, where also the reacted acid is recovered) (Balakrishnan et al., 2018). Several authors investigated the regeneration of pickling waste acid solutions by spray roasting (Bascone et al., 2016; Regel-Rosocka, 2010).

Membrane techniques are considered simple, effective and sustainable (Regel-Rosocka, 2010). These characteristics make them very attractive in acid recovery field, though their actual applicability strongly depends on high-performing membranes availability and cost. In this respect, diffusion dialysis (DD) is becoming popular thanks to the recent important advances in ion exchange membranes (IEMs) (Mondal et al., 2017). The main advantages of DD are: clean nature of the process, low installation and operating cost, operational simplicity and compatibility, low energy (Jung Oh et al., 2000; Luo et al., 2010; Xu et al., 2009)

In diffusion dialysis an anionic exchange membrane is used to achieve the separation of acid and salts. Due to the positive fixed charges present in the membrane, the transport of counter-ions (chlorides) is facilitated, whereas co-ions (iron cations, for instance) are rejected because of the electrostatic repulsion. However, also H^+ ions can diffuse through the anionic membrane, despite their positive charge, thanks to their little size and through the tunneling mechanism (Luo et al., 2011b; Strathmann, 2004; Xu et al., 2009). Therefore, the acid recovery and separation from salts occur.

Up to now, many authors have reported promising results for the recovery of HCl with DD. Among them, very few researchers studied the performances of Fumasep membranes (Palatý and Bendová, 2018). Research efforts have been devoted also to analyse how the acid concentration and the presence of metal salts (e.g. $FeCl_2$) can affect HCl recovery in DD. In particular, their effect on the diffusive permeability and the acid recovery have been quantitatively analysed (Jung Oh et al., 2000; Luo et al., 2013; Palatý and Bendová, 2009; Xu et al., 2009). Interestingly, only few researchers used very high concentrations of iron ions as in an industrial pickling waste (up to 150 g/l), when the leakage of cations through the anionic exchange membrane can be considerable (Xu et al., 2009).

In the DD process, the acid and iron salt diffusive permeability of the membrane is highly related to the mobility of all ionic species. Several researchers developed theoretical models to characterize transport phenomena in DD. Some important parameters, especially the permeability (P), have been defined and determined, both for the acid and the iron chloride transport, by carrying out experiments in batch (Davis, 2000; Kang et al., 2001; Luo et al., 2011a; Palatý and Bendová, 2009) and in continuous (Bendová et al., 2009; Davis, 2000; Kang et al., 2001) systems. Another important parameter, the water flux through the membrane, was also observed and poorly discussed only in a few cases (Davis, 2000; Jung Oh et al., 2000; Xu et al., 2009).

In the present work, a single-cell diffusion dialysis module was employed in order to study the effect of process parameters on the efficiency of HCl recovery, even in the presence of $FeCl_2$ at very high

concentrations, to simulate real industrial pickling waste conditions. In addition, a mathematical model able to simulate the process was developed and validated, providing an effective tool for the prediction of all the main process phenomena, from acid and salt flux to the water flux, and the simulation of real scale continuous or transitory operation.

2. Experimental

2.1 Materials

The solutions for diffusion dialysis experiments were prepared in laboratory from 37% HCl solution, $FeCl_2$ tetrahydrate (Carlo Erba reagents, purity ≥ 99%) and deionized water generated by a two-stage reverse osmosis (conductivity below 5 μS/cm). Na_2CO_3 (Carlo Erba reagents, purity ≥ 99.5%) was used for HCl titration. In all tests, the feed retentate solutions consist of HCl solutions from 0.1 to 3 M, or $FeCl_2$ solutions with Fe ions concentration from 50 to 150 g/l and 2 M HCl. The inlet diffusate stream is deionized water in tests performed to investigate the permeability of acid or the combined effect of acid and salt. Differently, for the investigation of iron diffusion through the membrane, a 0.1 M HCl concentration is used in the retentate and diffusate, in order to keep a low pH (thus avoiding iron precipitation phenomena in the retentate channel) and minimize acid flux between the two compartments.

The membrane adopted is a Fumasep type FAD from Fumatech GmbH and the main characteristics are reported in Table 1.

Table 1. Properties of Fumasep FAD type anion exchange membrane.

Item		Specifications
thickness (dry)	μm	70-80
electric resistance [a)]	Ω cm²	< 1

selectivity [b)]	%	> 90
stability	pH	< 9
ion exchange capacity	meq/g	> 1.5
specific conductance [c)]	mS/cm	> 13
weight per unit area	mg/cm^2	9-12
proton (H^+) transfer rate [d)]	$\mu mol\ min^{-1}\ cm^{-2}$	> 1500
Young's modulus [e)]	MPa	> 1000
tensile strength [e)]	MPa	> 40
elongation at break [e)]	%	> 15
bubble point test in water at T = 25 °C	bar	> 3

[a)] in Cl^- form in 0.5 M NaCl at T = 25°C, measured in standard measuring cell (through-plane)
[b)] determined from membrane potential measurement in a concentration cell 0.1/0.5 M KCl at T = 25°C
[c)] determined in Cl^- form in 0.5 NaCl at T =30°C
[d)] determined from pH potential measurement in a concentration cell 0.5 M HCl/0.5 M KCl at T = 25°C
[e)] determined by stress-strain measurement at T = 25°C and 50 % r.h., according to DIN EN 527-1

2.2 Diffusion dialysis set-up and experimental procedures

The diffusion dialysis module has a plate and frame configuration, consisting of two Plexiglas plates (20x20x2 cm^3) equipped with inlet-outlet manifolds, two spacers (thickness 270 μm) and an anion-exchange membrane (active area 10x10 cm^2) interposed between the two spacers. Retentate and diffusate solutions are circulated from/to in the same tanks and they are circulated through the DD module by two peristaltic pumps, thus realizing a batch operation mode. Figure 1 schematically illustrates the experimental set-up.

After the module assembly, a leakage test was performed by recirculating deionized water for 60 minutes and observing any internal or external leakage. Before each experiment, the apparatus was fully fed with an acidic solution (with an acid concentration equal to the average of the two feed solutions) in order to condition the membrane for 120 minutes. During experiments, pH and conductivity in the recirculation

tanks were measured by digital multi parameter pH/conductivity-meter (Hanna Instruments) and several samples were withdrawn to measure acid and iron concentration, the first one after 1 h, the others every two hours.

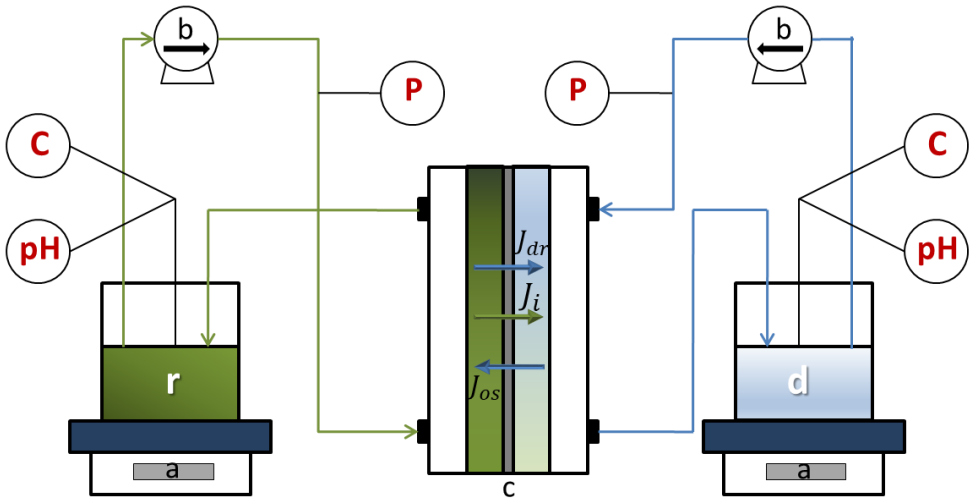

Fig. 1. Experimental set-up: (a) scales, (b) pumps, (c) DD module, (P) pressure gauges, (r) retentate tank, (d) diffusate tank. Osmotic (J_{os}), drag (J_{dr}) and i-component (J_i) fluxes through the membrane are indicated with arrows.

At the output of each pump, a pressure gauge is connected to the circuit, in order to monitor the pressure drops inside the stack. All the experiments were performed with a constant flow rate (48 ml/min) and at room temperature (20-25 °C). Preliminary test at lower flow rates were carried out and results were not significantly different, thus operating at the higher flow rate was preferred to reduce air bubbles trapping issues. Each experiment was repeated from 2 to 4 times in order to have a statistical relevance and to calculate the error bars reported in the graphs. Water flux was determined by weight measurements in the two tanks.

Parameters such as flux of *i*-species in solution, acid recovery and iron leakage are calculated from experimental results as a function of the test duration, by the closure of mass balances in the retentate or diffusate tanks:

$$J_i = -\frac{\Delta(V_r c_{i,r})}{A_m \Delta t} = -\frac{V_r|_t}{A_m}\left(\frac{c_{i,r}\big|_{t+\Delta t} - c_{i,r}\big|_t}{\Delta t}\right) - \frac{c_{i,r}\big|_t}{A_m}\left(\frac{V_r|_{t+\Delta t} - V_r|_t}{\Delta t}\right) \quad (1)$$

$$RR_{HCl}(\%) = \frac{V_d c_{HCl,d}\big|_{t+\Delta t} - V_d c_{HCl,d}\big|_t}{V_r^{in} c_{HCl,r}^{in}} x100 \quad (2)$$

$$Leakage_{FeCl_2}(\%) = \frac{V_d c_{FeCl_2,d}\big|_{t+\Delta t} - V_d c_{FeCl_2,d}\big|_t}{V_r^{in} c_{FeCl_2,r}^{in}} x100 \quad (3)$$

where RR_{HCl} and $Leakage_{FeCl_2}$represent the recovery ratio and leakage percentage of acid and $FeCl_2$ respectively.

In addition, the acid recovery efficiency (η_{HCl}) is defined as the ratio between the actual recovery of acid and the theoretical maximum recovery achievable when the two solutions reach the equilibrium (in the present case of equal feed tank volumes, corresponding to 50%).

$$\eta_{HCl}(\%) = \frac{RR_{HCl}}{RR_{HCl}^{max}} x100 \quad (4)$$

2.3 Analysis

The concentration of HCl was measured through conductivity measurements and verified by titration with a standard Na_2CO_3 solution. The concentration of Fe ions in solution was measured by spectrophotometric technique (Beckham DU 800 spectrophotometer) adding 1,10-phenanthroline and characterizing the samples at a λ of 510 nm.

3. Results and discussion

3.1 Effect of HCl concentration on acid permeability

The flux of acid at different initial concentrations was studied in order to determine the diffusive acid permeability. Several experiments were carried out with HCl at 0.1, 0.5, 1, 2 and 3 M at room

temperature using deionized water as draw solution. In Figure 2 (a), time variation of HCl concentration is reported in the retentate and diffusate tanks. Such variation can be ascribed to the presence of a diffusive acid flux through the membrane from the retentate to the permeate channel. This is reported in Figure 2 (b). In fact, according to the Fick's law, which relates the diffusive flux to the concentration gradient across the membrane, this flux decreases significantly along time due to the reduction in the concentration driving force, as also observed by Jung Oh et al. (2000). Moreover, also the permeability value is influenced by acid concentration (see section 5). In all these cases a recovery efficiency of almost 100% is reached after 24 hours of operation.

Finally, Figure 2 (c) reports the variation of volumes in the diffusate tank along time. Volume variation is related to the water flux through the membrane, which can be described with two terms (see Fig.1): an osmotic flux from the diffusate solution to the retentate one and a drag flux, which is the flux of water molecules associated with acid molecules passing from the retentate to the diffusate solution. The two counter acting effects lead to a diffusate volume decrease for the case of very low acid concentration (0.1 M), while it increases at higher concentrations (0.5–3 M). In fact, the drag flux prevails when acid concentrations are above a threshold limit of about 0.5 M, where the significant flux of acid leads to an important drag flux of water molecules, as already reported by some authors for the case at higher acid concentrations (Davis, 2000; Jung Oh et al., 2000).

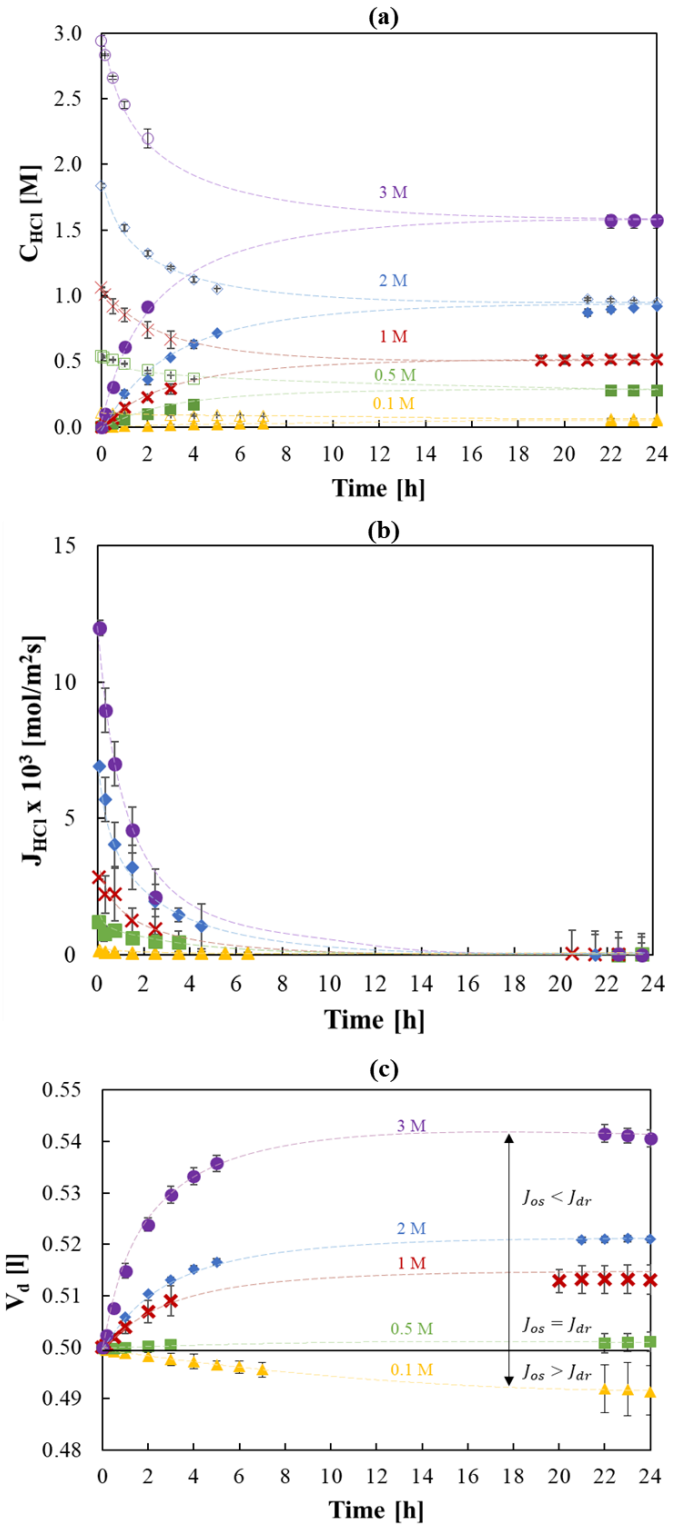

Fig. 2. (a) HCl concentration, (b) HCl flux and (c) Diffusate volume vs. time in the retentate (empty symbols) and in the diffusate (solid symbols). Initial HCl concentrations in the retentate: 0.1M (△), 0.5M (□), 1M (**X**), 2M (◊) and 3M (○). Flow rate: 48 ml min^{-1}. Retentate: HCl solution. Diffusate: deionized water.

3.2 Fe passage and its effect on HCl recovery

To evaluate the iron passage through the membrane, two solutions at the same HCl content (0.1 M) were used in the two channels in order to always keep an acidic pH. $FeCl_2$ was added in the retentate at different concentrations (namely 50, 100 and 150 g/l of Fe^{2+} ions). The experiments were performed with a flowrate of 48 ml/min in both the channels, at room temperature. As reported in Figure 3, a leakage from 2 to 12 g/l was detected after 7 hours increasing as the iron concentration increases.

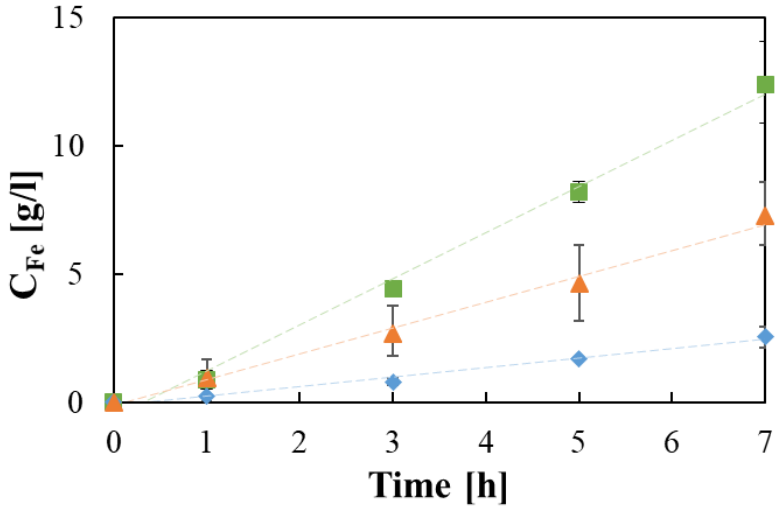

Fig. 3. Fe concentration vs. time in the diffusate. Initial Fe concentrations: 50 (♦), 100 (▲) and 150 (■) g/l. Initial acid concentration: 2M. Flow rate: 48 ml min^{-1}. Retentate: HCl and $FeCl_2$ solution. Diffusate: deionized water.

The effect of $FeCl_2$ concentration on the HCl recovery was also studied. As shown in Figure 4, for an initial iron concentration of 100 g/l, the acid recovery in the presence of iron in solution is higher compared to the one revealed in the absence of Fe. In fact, the acid concentration in the diffusate is higher than the one in the retentate (a cross can be observed in the figure), differently from the case without iron salt, when the maximum value of acid recovery is 50%. This is imputed to the so-called "salt effect", i.e. the addition of salt with the same anion of the acid causes an additional driving force for the diffusion of chlorides (Davis, 2000; Luo et al., 2011b; Xu et al., 2009), which leads to additional diffusion of protons in order to respect the electroneutrality of the system. Such phenomena are reflected

in acid recovery efficiency values above 100%, thus indicating the importance of salt effect in the HCl recovery process.

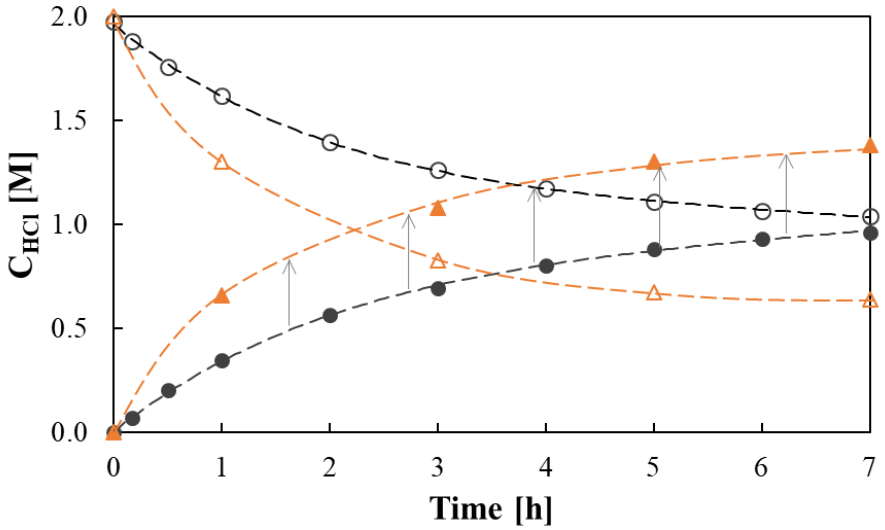

Fig. 4. Time variation of HCl concentration in the diffusate (solid symbols) and retentate (empty symbols). Initial Fe concentrations in retentate: 0 g/l (○) and 100 g/l (△). Initial acid concentration: 2M. Flow rate: 48 ml min^{-1}. Retentate: HCl and $FeCl_2$ solution. Diffusate: deionized water.

Moreover, it was observed that the HCl recovery increases by increasing $FeCl_2$ concentration, keeping the initial HCl concentration at a constant value (2 M). Of course, even though the acid permeation increases, also the Fe leakage through the membrane increases, causing a loss of membrane efficiency in co-ions rejection. The two performance parameters, acid recovery and iron leakage, increase from 50 to 75% and 7%, respectively, by increasing initial Fe ions concentration from 50 to 150 g/l, as shown in Figure 5, which results in an acid recovery efficiency of 150%. Concerning the water flux, diffusate volume profiles are reported in Figure 6.

As shown, the drag flux initially prevails, then a net water flux from the diffusate to the retentate is observed, thus indicating an overall prevalent osmotic flux. A critical time, t*, can be identified when drag and osmotic fluxes are equivalent. As expected, t* decreases when increasing $FeCl_2$ concentration, due to the stronger effect of salts in determining the osmotic pressure increase in the retentate.

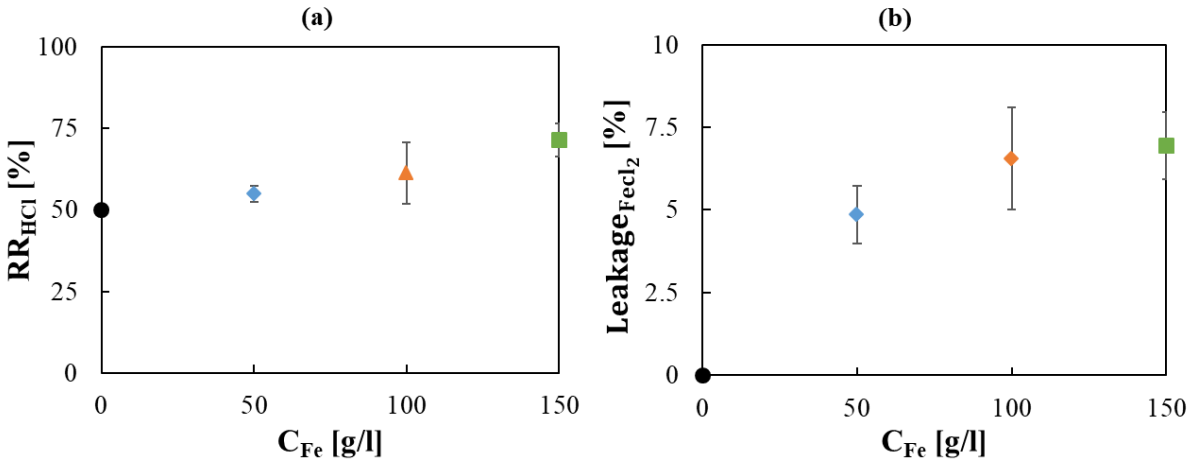

Fig. 5. (a) HCl Recovery Ratio and (b) $FeCl_2$ leakage percentage vs. initial Fe concentration in the retentate: 0 (●) 50 (♦), 100 (▲) and 150 g/l (■). Initial acid concentration: 2M. Flow rate: 48 ml min^{-1}. Retentate: HCl and $FeCl_2$ solution. Diffusate: deionized water.

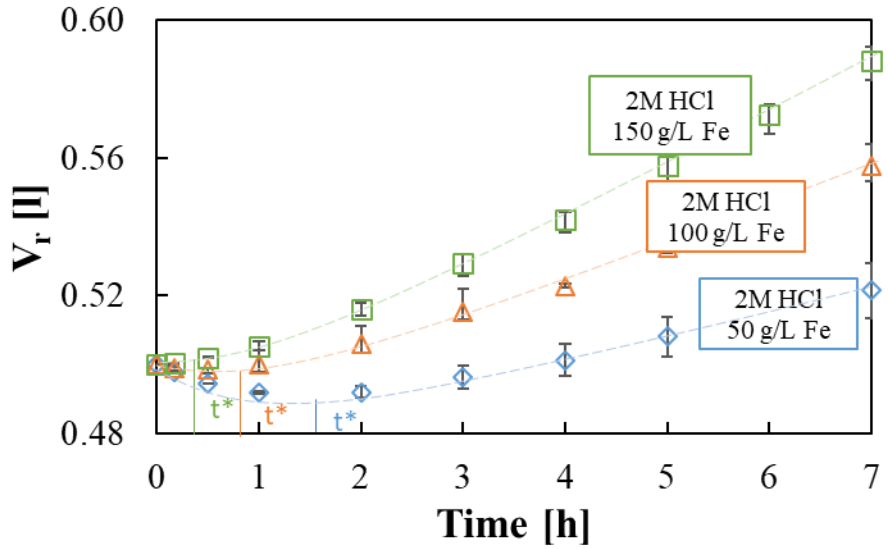

Fig. 6. Retentate volume vs. time. Initial Fe concentrations: 50 (◊), 100 (△) and 150 (□) g/l. Initial acid concentration: 2M. Flow rate: 48 ml min^{-1}. Retentate: HCl and $FeCl_2$ solution. Diffusate: deionized water.

4. Model for Diffusion Dialysis

A model was developed in order to simulate the Diffusion Dialysis process in steady-state and batch operation. For that purpose, the model includes steady-state spatial differential mass balance equations (section 4.1) with a 1-dimensional spatial discretization of the DD unit along channels and time

differential equations describing the variation of concentration and of volume in the two feed tanks during batch operations (section 4.2).

4.1 Spatial differential model equations

Figure 7 shows the sketch of a countercurrent module of length z_{ch} and membrane area A_m.

Since the concentration of the i-component in I is higher than in II, a mass transport from I to II occurs. Thus, the concentration of the i-component in the retentate side decreases and, conversely, in the diffusate side it increases along the flow direction.

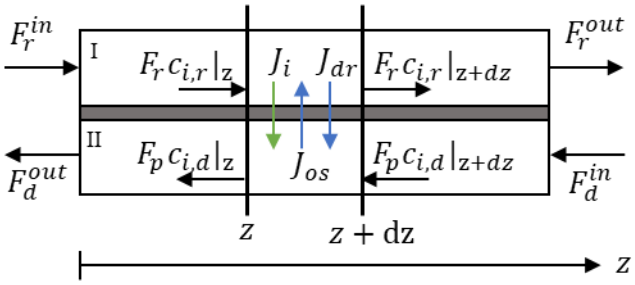

Fig. 7. Schematic representation of the discretized domain of the DD unit, indicating the main variables.

Assuming steady-state conditions and considering diffusion and convection mass transport, the variation of concentration along z in the two channels can be derived from the mass balance on the differential volume between *z* and *z+dz* (only the equations for the retentate are reported for the sake of brevity):

$$F_r c_{i_r}\big|_z = F_r c_{i_r}\big|_{z+dz} + J_i dA_m \tag{5}$$

$$dA_m = dz w_{ch} \tag{6}$$

$$\frac{dF_r c_{i_r}}{dz} = -J_i w_{ch} \tag{7}$$

$$\frac{dF_r}{dz} = \sum_i \frac{dF_r c_{i_r}}{dz} \frac{PM_i}{\rho_r} \tag{8}$$

where c_{i_r} is the bulk concentration of the *i*-component in the retentate side; F_r is the volumetric flow rate in the retentate channel; J_i is the molar flux of the *i*-component through the membrane; dA_m is the

differential membrane area; w_{ch} is the channel width; PM_i and ρ_r are molecular weight and density of the retentate solution, respectively.

The boundary conditions for the two feeds are:

$$z = 0 \qquad c_{i,r} = c_{i,r}^{in} \tag{9}$$

$$z = z_{ch} \qquad c_{i,d} = c_{i,d}^{in} \tag{10}$$

The flux of the i-component is controlled by resistances in series i.e. from the bulk of retentate to the membrane interface (Eq.11), across the membrane (Eq. 12) and from the membrane interface at the diffusate side to the bulk of the diffusate (Eq. 13):

$$J_i = k_{i,r}\left(c_{i,r} - c_{i,r}^{int}\right) \tag{11}$$

$$J_i = P_i\left(c_{i_r}^{int} - c_{i_d}^{int}\right) \tag{12}$$

$$J_i = k_{i,d}\left(c_{i,d}^{int} - c_{i,d}\right) \tag{13}$$

where $k_{i,r}$ and $k_{i,d}$ are the mass transport coefficients for the *i*-component in retentate and diffusate channels, respectively; $c_{i,r}$ and $c_{i,d}$ are the bulk concentrations in the retentate and diffusate solutions; P_i is the permeability of the *i*-component through the membrane; $c_{i,r}^{int}$ and $c_{i,d}^{int}$ are the solution concentrations at the retentate and diffusate membrane interface, respectively.

To determine the mass transport coefficients, data from literature were used (Gurreri et al., 2014; Perry and Green, 2008). In particular, a Sherwood number in a laminar regime, in forced convection and for planar configuration was derived as:

$$Sh_r = \left(-1.48110^{-7}{Re_r}^5 + 3.73910^{-5}{Re_r}^4 - 0.003253{Re_r}^3 + 0.1118{Re_r}^2 + 0.1348Re_r + 6.9536\right)\left(\frac{Sc_r}{600}\right)^{0.5} \tag{14}$$

where Sh_r, Re_r and Sc_r are dimensionless numbers:

$$Sh_r = \frac{k_{i_r} D_{eq}}{\mathcal{D}} \qquad Re_r = \frac{\rho_r v_r D_{eq}}{\mu_r} \qquad Sc_r = \frac{\mu_r}{\rho_r \mathcal{D}_i} \tag{15}$$

where v_r is the fluid linear velocity in the retentate channel, μ_r is dynamic viscosity of the fluid in the retentate channels, $\mathcal{D}_i$ is the mass diffusivity of the i-component and D_{eq} is the hydraulic diameter defined as:

$$D_{eq} = \frac{4 s_{ch} w_{ch}}{2(s_{ch} + w_{ch})} \tag{16}$$

where s_{ch} is channel thickness.

A single equation transport can be derived (Eq. 17), where an overall mass transfer coefficient of the i-component (U_i) can be used (Eq. 18) to express the flux as function of the bulk concentration.

$$J_i = U_i(c_{i,r} - c_{i,d}) \tag{17}$$

$$U_i = \left(\frac{1}{k_{i,r}} + \frac{1}{P_i} + \frac{1}{k_{i,d}}\right)^{-1} \tag{18}$$

The permeability coefficient (P_i) takes into account the absorption coefficient and the membrane permeability itself.

Transport of water through the membrane also affects process performances. Water flux was considered in the model as the sum of the osmotic and drag fluxes, where the osmotic flux depends on the osmotic pressure driving force, while the drag flux is related to the total water molecules associated to ions transport (Eq. 19-21).

$$J_w = J_{os} + J_{dr} \tag{19}$$

$$J_{os} = P_{os} RT \sum v_i (c_{i,r} - c_{i,d}) \tag{20}$$

$$J_{dr} = \sum_i \beta_i J_i \tag{21}$$

where J_w, J_{os} and J_{dr} are the total, osmotic and drag water fluxes, respectively, P_{os} is the osmotic permeability of the membrane and β_i is the hydration number of species i. Hydration numbers equal to 1 for protons, 6 for chlorides and 6 for the iron cations were considered (Lundberg et al., 2007).

The flux of HCl through the membrane is affected by the presence of $FeCl_2$ in solution. As reported by some authors (Davis, 2000; Palatý and Bendová, 2009), the total acid flux (J_{HCl}^{tot}) can be considered as the sum of two terms, one dependent on the actual acid concentration difference and the other one related to the presence of additional chlorides from the iron salt (Eq. 22):

$$J_{HCl}^{tot} = U_{HCl}\left(c_{HCl,r} - c_{HCl,d}\right) + U_{HCl}^{S}\left(c_{FeCl_2,r} - c_{FeCl_2,d}\right) \tag{22}$$

where J_{HCl}^{tot} is the hydrochloric acid molar flux through the membrane, U_{HCl}^{S} is the secondary overall mass transfer coefficient related to the presence of iron salts, and $c_{FeCl_2,r}$ and $c_{FeCl_2,d}$ are the concentrations of the salt in the retentate and diffusate solutions, respectively.

Considering Eqs 11-13, 19-21, it is possible to derive the flux of $FeCl_2$ as:

$$J_{FeCl_2} = U_{FeCl_2}\left(c_{FeCl_2,r} - c_{FeCl_2,d}\right) \tag{23}$$

In order to estimate the efficiency of the process, two important parameters are evaluated: the acid recovery ratio (RR_{HCl}) and the iron leakage through the membrane ($Leakage_{FeCl_2}$).

The acid recovery ratio (RR_{HCl}) is calculated as:

$$RR_{HCl}\ (\%) = \frac{F_d^{out} c_{HCl,d}^{out} - F_d^{in} c_{HCl,d}^{in}}{F_r^{in} c_{HCl,r}^{in}} x100 \tag{24}$$

where the superscripts *in* and *out* indicate the inlet and outlet from the DD channel, respectively.

The iron leakage ($Leakage_{FeCl_2}$) is calculated as:

$$Leakage_{FeCl_2}(\%) = \frac{F_d^{out} c_{FeCl_2,d}^{out} - F_d^{in} c_{FeCl_2,d}^{in}}{F_r^{in} c_{FeCl_2,r}^{in}} x100 \quad (25)$$

4.2 Time-dependent model equations

In order to simulate the time-dependent variations of concentrations and volumes of the two tanks in the batch operation mode, the model also includes a dynamic part consisting of time-differential equations for the volume and concentration of the feed tanks (see Fig. 8).

$$\frac{d\rho_r V_r}{dt} = \rho_r^{in} F_r^{in,Dyn} - \rho_r^{out} F_r^{out,Dyn} \quad (26)$$

$$\frac{dV_r c_{i,r}^{tank}}{dt} = F_r^{in,Dyn} c_{i,r}^{in,Dyn} - F_r^{out,Dyn} c_{i,r}^{out,Dyn} \quad (27)$$

where $F_r^{in,Dyn}$ and $F_r^{out,Dyn}$ represent the inlet/outlet volumetric flowrates in the retentate tank, equal to the outlet/inlet retentate stream in the DD unit, respectively. In the same way, $c_{i,r}^{in,Dyn}$ and $c_{i,r}^{out,Dyn}$ are the inlet/outlet concentrations in the retentate tank, equal to the outlet/inlet concentrations retentate stream in the DD unit, respectively, while $c_{i,r}^{tank}$ is the concentration of the *i*-component in the retentate tank. In all cases, perfect mixing is assumed in the tanks, thus:

$$c_{i,r}^{out,Dyn} = c_{i,r}^{tank} \quad (28)$$

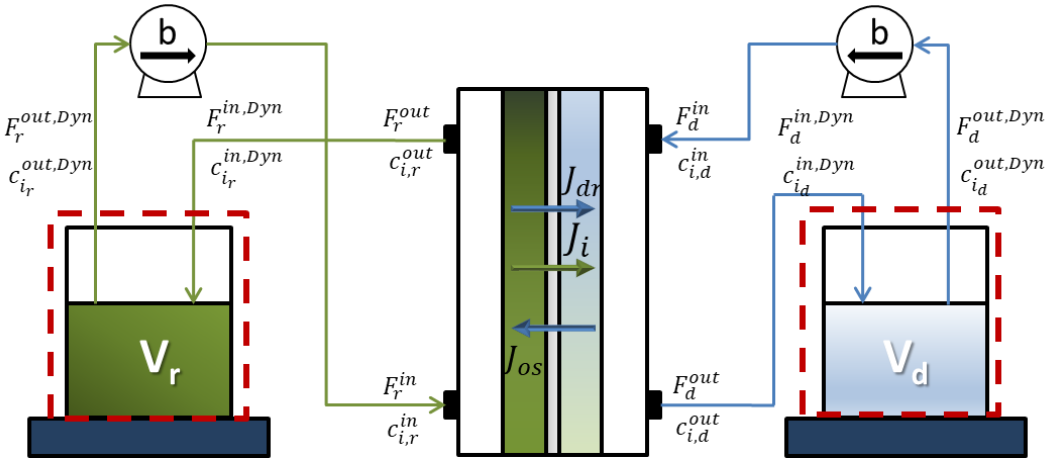

Fig. 8. Schematics of the control volumes in the DD set-up for the dynamic section of the model

Volume and concentration variations in the diffusate tank are calculated from the closure of mass balance equations.

The overall concentration and volume profiles were determined by numerically implementing the model according to the algorithm shown in Fig.9.

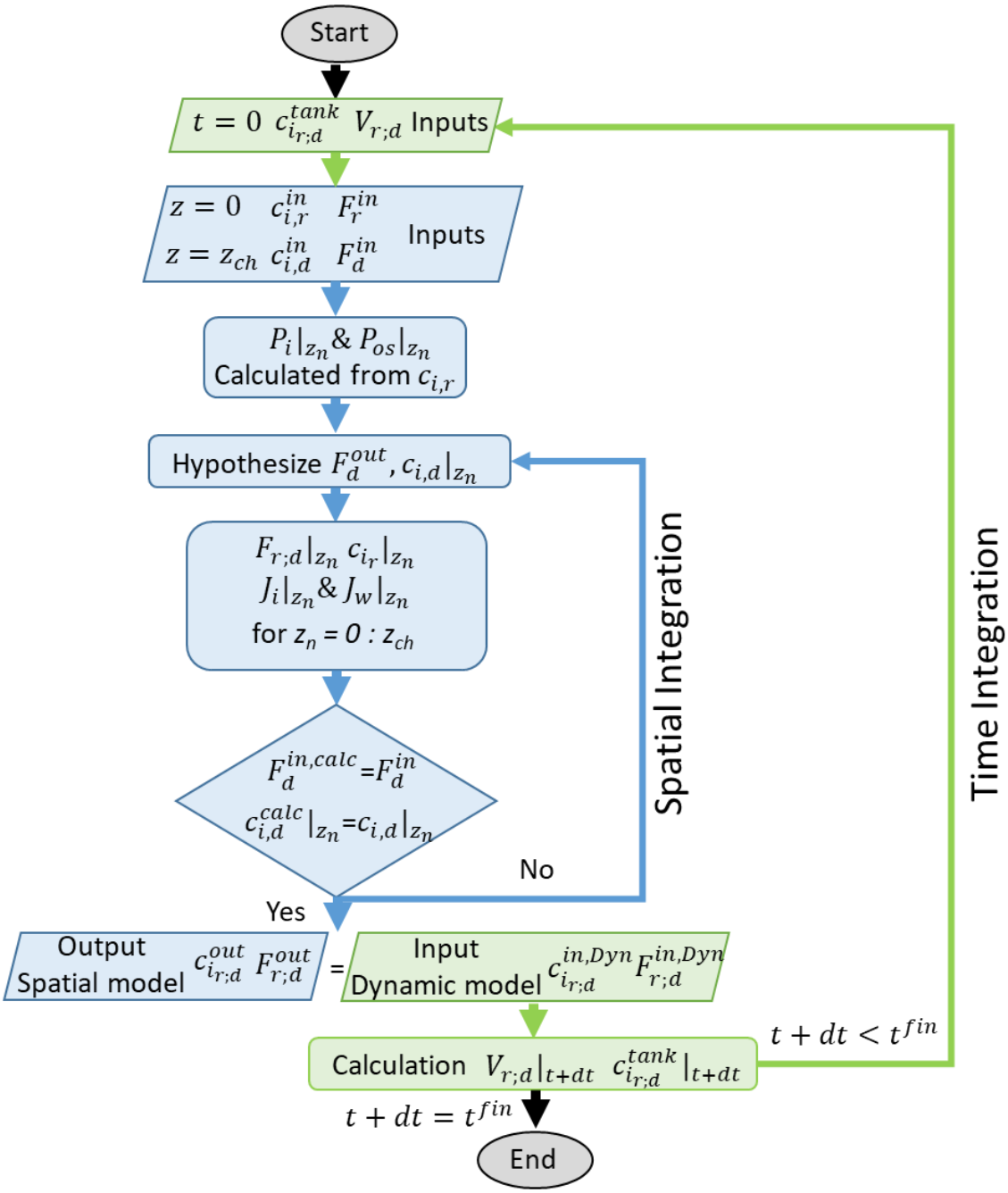

Fig. 9. Algorithm for the numerical implementation of the spatial-time dependent in diffusion dialysis model

Values of permeability were determined through a calibration procedure (presented in section 5) and are related to the acid concentration in the retentate solution.

5. Model calibration and validation

5.1 Model calibration

Calibration permeability values of the membrane with respect to the acid, salt and water diffusion have been related to the concentration of the acid and salt in the feed solution using experimental data. For each experiment a good fitting between experimental and model data was obtained by using linear correlations for the acid (P_{HCl}) and for water (P_{os}) permeability as a function of the acid concentration in the retentate. By way of example, the comparison between experimental data and model prediction is reported in Figure 10 for the 2M HCl test.

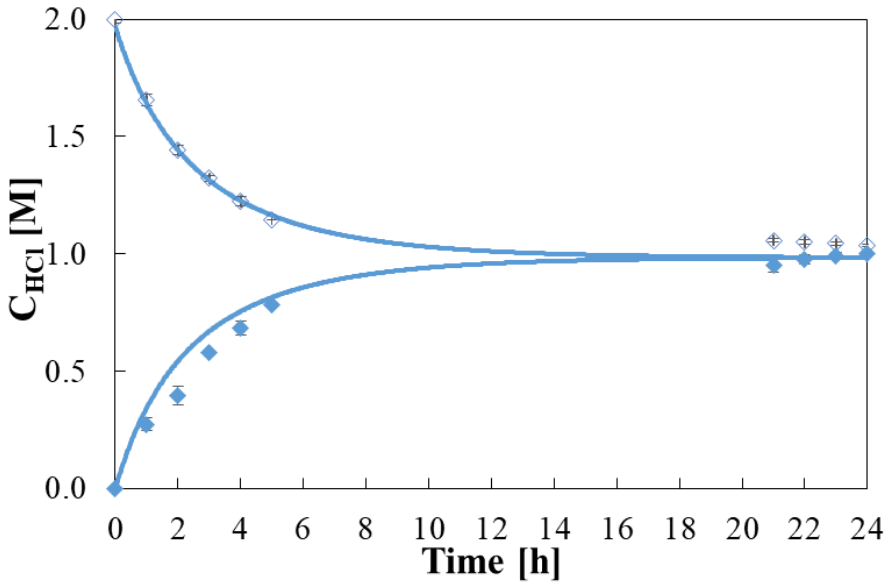

Fig. 10. Comparison between experimental data in the retentate (empty symbols) and in the diffusate (solid symbols) and model predictions (continuous line) for 2M HCl test. Flow rate: 48 ml min^{-1}. Retentate: HCl solution. Diffusate: deionized water.

Therefore, all these linear trends were plot in a graph (Fig. 11) in order to obtain a unique correlation relating acid permeability values to the acid concentration in the retentate tank, as reported below:

$$P_{HCl} = 3.21 \cdot 10^{-7} c_{r,HCl}^3 - 1.93 \cdot 10^{-6} c_{r,HCl}^2 + 4.11 \cdot 10^{-6} c_{r,HCl} + 6.61 \cdot 10^{-7} \quad (29)$$

As previously mentioned in section 3, the diffusive permeability to the acid is strongly affected by the acid concentration.

In fact, as reported in Figure 11 (a), it increases as HCl concentration increases in the whole range investigated.

In a similar way, osmotic permeability coefficients were obtained experimentally as an increasing function of the acid concentration (Figure 11 (b)) as:

$$P_{os} = 1.7 \cdot 10^{-6} c_{r,HCl} + 6.3 \cdot 10^{-6} \quad (30)$$

Finally, the $FeCl_2$ leakage permeability coefficient was calibrated according to a similar procedure. However, differently from the acid, a constant value for each test was considered.

As shown in Figure 11 (c), also $FeCl_2$ diffusive permeability increases as the salt concentration increases, though, as expected, permeability of the salt is 10 times lower than for the acid:

$$P_{FeCl_2} = -1.87 \cdot 10^{-8} c_{r,FeCl_2}^2 + 1.17 \cdot 10^{-7} c_{r,FeCl_2} + 3 \cdot 10^{-8} \quad (31)$$

As already described in Eq. 23, in order to consider the salt effect, acid permeation in the presence of $FeCl_2$ was modelled. In this case, the U_{FeCl_2} coefficient was also experimentally obtained, showing a linear dependence on the acid concentration:

$$U_{FeCl_2} = 2.6 \cdot 10^{-6} c_{r,HCl} + 9.95 \cdot 10^{-8} \quad (32)$$

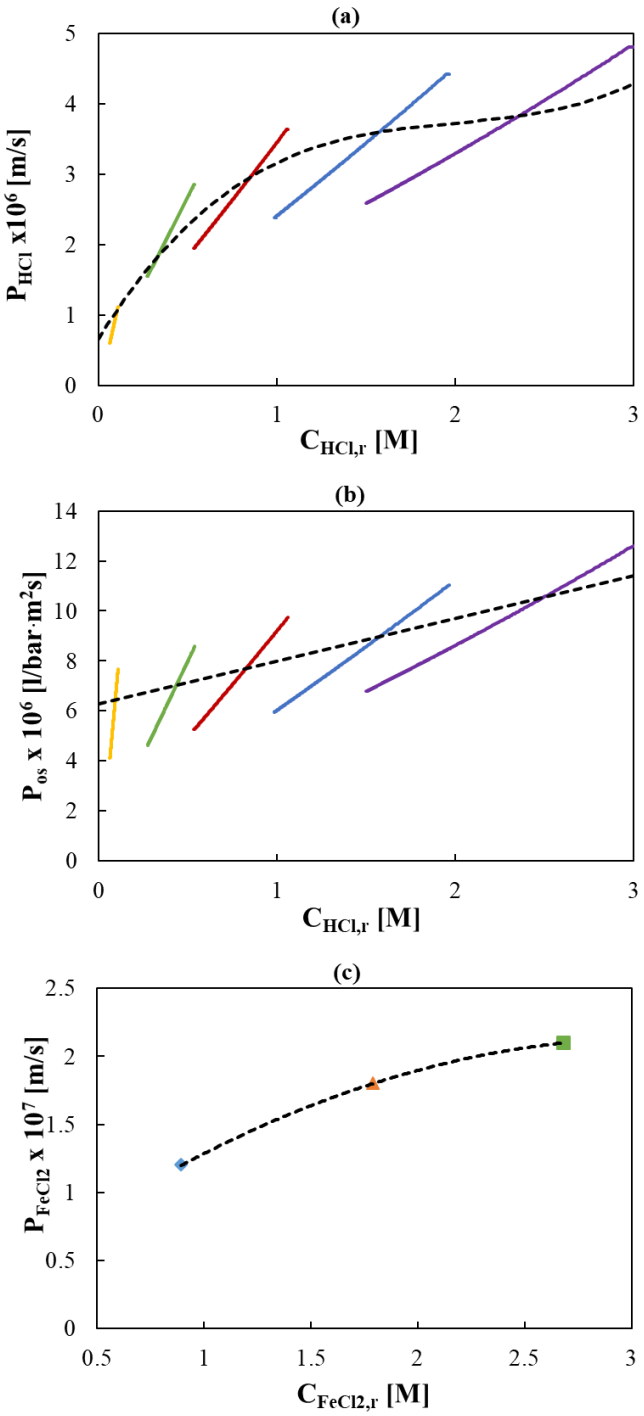

Fig. 11. Linear correlations (continuous line) and overall trend (dotted curve) of the acid diffusive permeability (a) and osmotic permeability (b) obtained for the model calibration as a function of HCl concentration in the retentate; values and overall trend (dotted curve) of the iron diffusive permeability obtained for the model calibration as a function of $FeCl_2$ concentration in the retentate (c).

In order to compare diffusive permeability ranges obtained in this work with the values reported in literature for other membranes, a summary table was prepared (Table 2). A comparison between acid permeabilities indicates that Fumasep membrane behaves better than most other AEMs tested, although iron salt permeability is slightly higher.

Table 2. Comparison of diffusive permeability among different membranes.

Membrane AEM	Concentration Range	Operation Configuration	P_{HCl} ($10^{-6}\frac{m}{s}$)	P_{FeCl_2} ($10^{-7}\frac{m}{s}$)	Ref
Fumasep FAD	0.1-3 M HCl 0.9-2.7 M $FeCl_2$	Batch recirculation	1-4	1-2	This work
Fumasep FAD	0.2-2 M HCl	Two compartment stirred cells	3.7-13.4	-	Palatý and Bendová, 2018
Neosepta AFN	4 M HCl 0.26 M $FeCl_2$	Dialyzer Stack	2.1	0.14	Jung Oh et al., 2000
DF-120	1.28 M HCl 0.22 M $FeCl_2$	Two compartment stirred cells	3	1.4	Luo et al., 2010
PPO-SiO_2	1.28 M HCl 0.22 M $FeCl_2$	Two compartment stirred cells	1.5-3	0.7	Luo et al., 2010

5.2 Model validation

The model was validated by comparison with all experimental trends observed. As an example, Figure 12 reports a comparison between predicted and experimental trends for some of the investigated cases. Instead, in Figure 13 a comparison of experimental data and model predictions is reported for all the investigated cases.

In all cases a good agreement is shown between model and experiments.

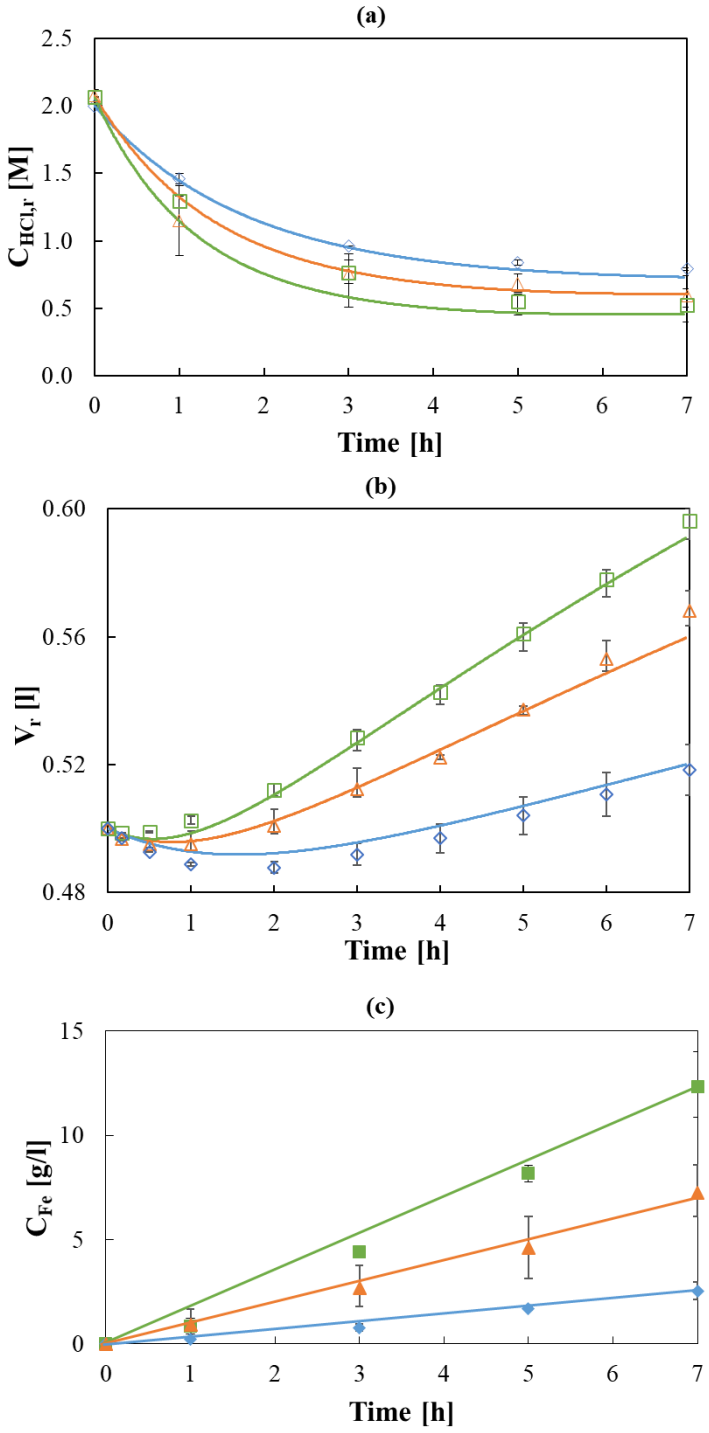

Fig. 12. HCl concentration in retentate (a), retentate volume (b) and Fe concentration in diffusate (c) vs. time. Initial Fe concentrations: 50 (◊,♦), 100 (△,▲) and 150 (□,■) g/l. Initial acid concentrations: 2M. Flow rate: 48 ml min^{-1}. Retentate solution: deionized water, HCl, $FeCl_2$. Diffusate solution: deionized water. Theoretical curves (—) obtained by using the model.

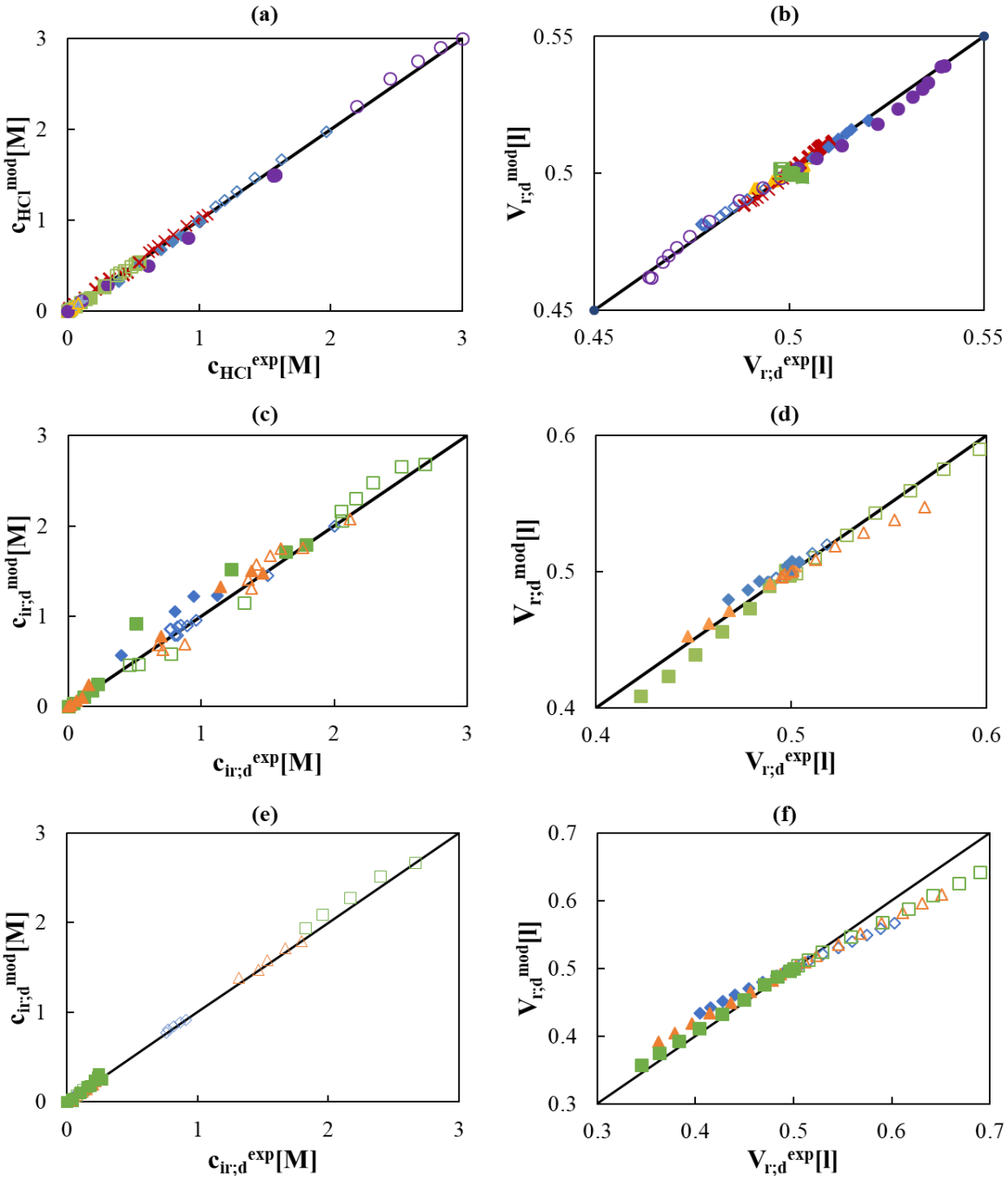

Fig. 13. Comparison of experimental and predicted values of concentration of species and tanks volumes in retentate and diffusate compartments. (a)&(b) tests with only HCl at 0.1M (▲), 0.5M (■), 1M (X), 2M (♦), 3M (●); (c)&(d) tests with initial HCl at 2M and Fe at 50 (♦), 100 (▲), 150 (■) g/l; (e)&(f) tests with initial HCl at 0.1M and Fe at 50 (♦), 100 (▲), 150 (■) g/l.

6. Conclusions

HCl recovery from pickling solutions by Diffusion Dialysis was investigated, highlighting the main effects of operating conditions on process performance. Acid flux was significantly enhanced by higher acid concentration in the retentate due to a larger driving force and a higher value of acid diffusive permeability through the membrane. The effect of the iron (II) chloride on the acid recovery was also investigated, indicating how the acid flux is enhanced as the $FeCl_2$ concentration increases, due to the "salt effect", reaching an acid recovery efficiency over 100%, despite the batch configuration adopted. Also the $FeCl_2$ diffusive permeability increases as the Fe concentration increases. However, the highest leakage detected is only 7% in the most severe conditions. A detailed analysis of osmotic and drag water flux in DD operation is presented. For pure HCl tests, at low HCl concentrations, the osmotic flux prevails, whereas at higher concentrations a net water flux in the opposite direction is observed due to the presence of a drag flux, related to the water molecules associated to ions transported through the membrane. Conversely, in the presence of Fe ions, the osmotic flux always dominates water transport phenomena.

The whole process was mathematically described within a time/space distributed-parameters model implemented and adopted as a process simulator. The model was calibrated and fully validated using the available experimental data in the wide range of acid and iron concentration investigated (0.1-3 M and 50 – 150 g/l, respectively), providing a powerful tool for the simulation and optimisation of DD operation in transient and steady-state operation.

Acknowledgements

This work was financially supported by EU within the ReWaCEM project (Resource recovery from industrial Wastewater by Cutting Edge Membrane technologies) – Horizon 2020 program, Grant Agreement no. 723729.

The authors are greeting to DEUKUM GmbH and Fumatech GmbH for supporting during the DD stack assembly and supplying the AEM membranes.

Nomenclature and acronyms

AEM		Anion Exchange Membrane
DD		Diffusion Dialysis
IEMs		Ion Exchange Membranes
A	$[m^2]$	area
c	$\left[\frac{mol}{l}\right]$	molar concentration
D	$[m]$	hydraulic diameter
$\mathcal{D}$	$\left[\frac{m^2}{s}\right]$	mass diffusivity
F	$\left[\frac{l}{s}\right]$	volumetric flow rate
J_i	$\left[\frac{mol}{m^2 \cdot s}\right]$	molar flux
$J_w; J_{os}; J_{dr}$	$\left[\frac{l}{m^2 \cdot s}\right]$	volumetric flux
k	$\left[\frac{m}{s}\right]$	mass transport coefficient
P_i	$\left[\frac{m}{s}\right]$	diffusive permeability
PM	$\left[\frac{g}{mol}\right]$	molecular weight

P_{os}	$\left[\frac{l}{bar \cdot m^2 \cdot s}\right]$	osmotic permeability
R	$\left[\frac{l \cdot bar}{K \cdot mol}\right]$	gas costant
Re	[-]	Reynolds number
RR	[%]	recovery ratio
s	$[m]$	thickness
Sc	[-]	Schmidt number
Sh	[-]	Sherwood number
T	[K]	temperature
U	$\left[\frac{m}{s}\right]$	overall mass transfer coefficient
V	$[l]$	volume
v	$\left[\frac{m}{s}\right]$	linear velocity
w	$[m]$	width
z	$[m]$	length
β	[-]	hydration number
η	[%]	recovery efficiency
μ	$[Pa \cdot s]$	dynamic viscosity
ρ	$\left[\frac{g}{l}\right]$	density

Subscripts and superscripts

calc	calculated
ch	channel
d	diffusate
Dyn	dynamic

dr	drag
eq	equivalent
fin	final
i	component *i*, i.e., HCl, $FeCl_2$
in	inlet
int	interface
m	membrane
max	maximum
n	discretization number
os	osmotic
out	outlet
r	retentate
s	salt
t	time
tank	tank
tot	total
w	water
I	compartment I
II	compartment II

References

Balakrishnan, M., Batra, R., Batra, V.S., Chandramouli, G., Choudhury, D., Hälbig, T., Ivashechkin, P., Jain, J., Mandava, K., Mense, N., Nehra, V., Rögener, F., Sartor, M., Singh, V., Srinivasan, M.R., Tewari, P.K., 2018. Demonstration of acid and water recovery systems: Applicability and operational challenges in Indian metal finishing SMEs. J. Environ. Manage. 217, 207-213. https://doi.org/10.1016/j.jenvman.2018.03.092

Bascone, D., Cipollina, A., Morreale, M., Randazzo, S., Santoro, F., Micale, G., 2016. Simulation of a regeneration plant for spent pickling solutions via spray roasting. Desalin. Water Treat. 57, 23405-23419. https://doi.org/10.1080/19443994.2015.1137146

Bendová, H., Palatý, Z., Žáková, A., 2009. Continuous dialysis of inorganic acids: permeability of Neosepta-AFN membrane. Desalination 240, 333–340. https://doi.org/10.1016/j.desal.2007.10.096

Davis, T., 2000. II / MEMBRANE SEPARATIONS / Diffusion Dialysis. Nano 1693–1701. https://doi.org/10.1016/B0-12-226770-2/05751-3

Gurreri, L., Tamburini, A., Cipollina, A., Micale, G., Ciofalo, M., 2014. CFD prediction of concentration polarization phenomena in spacer-filled channels for reverse electrodialysis. J. Memb. Sci. 468, 133-148. https://doi.org/10.1016/j.memsci.2014.05.058

Jung Oh, S., Moon, S.H., Davis, T., 2000. Effects of metal ions on diffusion dialysis of inorganic acids. J. Memb. Sci. 169, 95–105. https://doi.org/10.1016/S0376-7388(99)00333-6

Kang, M.S., Yoo, K.S., Oh, S.J., Moon, S.H., 2001. A lumped parameter model to predict hydrochloric acid recovery in diffusion dialysis. J. Memb. Sci. 188, 61–70. https://doi.org/10.1016/S0376-7388(01)00372-6

Lundberg, D., Ullström, A.S., D'Angelo, P., Persson, I., 2007. A structural study of the hydrated and the dimethylsulfoxide, N,N′-dimethylpropyleneurea, and N,N-dimethylthioformamide solvated iron(II) and iron(III) ions in solution and solid state. Inorganica Chim. Acta 360, 1809–1818. https://doi.org/10.1016/j.ica.2006.09.014

Luo, J., Wu, C., Wu, Y., Xu, T., 2013. Diffusion dialysis of hydrochloric acid with their salts: Effect of co-existence metal ions. Sep. Purif. Technol. 118, 716–722. https://doi.org/10.1016/j.seppur.2013.08.014

Luo, J., Wu, C., Wu, Y., Xu, T., 2011a. Diffusion dialysis processes of inorganic acids and their salts: The permeability of different acidic anions. Sep. Purif. Technol. 78, 97–102. https://doi.org/10.1016/j.seppur.2011.01.028

Luo, J., Wu, C., Wu, Y., Xu, T., 2010. Diffusion dialysis of hydrochloride acid at different temperatures using PPO-SiO_2 hybrid anion exchange membranes. J. Memb. Sci. 347, 240-249.

https://doi.org/10.1016/j.memsci.2009.10.029

Luo, J., Wu, C., Xu, T., Wu, Y., 2011b. Diffusion dialysis-concept, principle and applications. J. Memb. Sci. 366, 1-16. https://doi.org/10.1016/j.memsci.2010.10.028

Mondal, A.N., Cheng, C., Khan, M.I., Hossain, M.M., Emmanuel, K., Ge, L., Wu, B., He, Y., Ran, J., Ge, X., Afsar, N.U., Wu, L., Xu, T., 2017. Improved acid recovery performance by novel Poly(DMAEM-co-γ-MPS) anion exchange membrane via diffusion dialysis. J. Memb. Sci. 525, 163–174. https://doi.org/10.1016/j.memsci.2016.10.042

Palatý, Z., Bendová, H., 2018. Permeability of a Fumasep-FAD membrane for selected inorganic acids. Chem. Eng. Technol. 41, No.2, 385-391. https://doi.org/10.1002/ceat.201700595

Palatý, Z., Bendová, H., 2009. Separation of HCl + $FeCl_2$ mixture by anion-exchange membrane. Sep. Purif. Technol. 66, 45–50. https://doi.org/10.1016/j.seppur.2008.11.026

Perry, R.H., Green, D.W., 2008. Perry's Chemical Engineers' Handbook, McGraw-Hill. https://doi.org/10.1017/CBO9781107415324.004

Regel-Rosocka, M., 2010. A review on methods of regeneration of spent pickling solutions from steel processing. J. Hazard. Mater. 177, 57-69. https://doi.org/10.1016/j.jhazmat.2009.12.043

Strathmann, H., 2004. Electrochemical and Thermodynamic Fundamentals, in: Ion-Exchange Membrane Separation Processes. 9, 23-88. https://doi.org/10.1016/S0927-5193(04)80033-0

Xu, J., Lu, S., Fu, D., 2009. Recovery of hydrochloric acid from the waste acid solution by diffusion dialysis. J. Hazard. Mater. 165, 832-837. https://doi.org/10.1016/j.jhazmat.2008.10.064